UC San Diego

UC San Diego Previously Published Works

Title

A simple model of intrinsic rotation in high confinement regime tokamak plasmas

Permalink

https://escholarship.org/uc/item/38w1z5cq

Journal

Physics of Plasmas, 17(3)

ISSN

1070-664X

Authors

Gürcan, ÖD
Diamond, PH
McDevitt, CJ
et al.

Publication Date

2010-03-01

DOI

10.1063/1.3339909

Copyright Information

This work is made available under the terms of a Creative Commons Attribution-NonCommercial-NoDerivatives License, availalbe at https://creativecommons.org/licenses/by-nc-nd/4.0/

Peer reviewed

eScholarship.org Powered by the California Digital Library
University of California

A simple model of intrinsic rotation in high confinement regime tokamak plasmas

Ö. D. Gürcan,[1,a)] P. H. Diamond,[2] C. J. McDevitt,[2] and T. S. Hahm[3]
[1]*Laboratoire de Physique des Plasmas, Ecole Polytechnique, CNRS, 91128 Palaiseau Cedex, France*
[2]*Center for Astrophysics and Space Sciences, University of California, San Diego, 9500 Gilman Dr., La Jolla, California 92093-0424, USA*
[3]*Princeton Plasma Physics Laboratory, Princeton University, Princeton, New Jersey 08543-0451, USA*

(Received 6 November 2009; accepted 8 February 2010; published online 26 March 2010)

A simple unified model of intrinsic rotation and momentum transport in high confinement regime (H-mode) tokamak plasmas is presented. Motivated by the common dynamics of the onset of intrinsic rotation and the L-H transition, this simple model combines $E\times B$ shear-driven residual stress in the pedestal with a turbulent equipartition pinch to yield rotation profiles. The residual stress is the primary mechanism for buildup of intrinsic rotation in the H-mode pedestal, while the pinch drives on-axis peaking of rotation profiles. Analytical estimates for pedestal flow velocities are given in terms of the pedestal width, the pedestal height, and various model parameters. The predicted scaling of the toroidal flow speed with pedestal width is found to be consistent with the International Tokamak Physics Activity database global scaling of the flow speed on-axis with the total plasma stored energy. © *2010 American Institute of Physics*. [doi:10.1063/1.3339909]

I. INTRODUCTION

A. Motivation

Understanding angular momentum transport in magnetic confinement devices is now a well-recognized problem. The recent observations of "spontaneous" or "intrinsic" rotation in various machines,[1–4] and the clear scaling trends observed with different heating schemes for the high confinement (H) mode,[1,4,5] and trends that have been identified during L-H transition,[6] make it an interesting but challenging subject of study.

Rice's scaling (i.e., $v_\phi \propto \Delta W_p/I_p$),[1] and consistency of the H-mode intrinsic rotation trends point to the existence of a direct link between H-mode intrinsic rotation and pedestal physics. Such a link is consistent with the idea that an $E\times B$ shear-driven residual stress may be responsible for the intrinsic rotation phenomenon.[7] It is also interesting to note that several authors seems to have independently come to the conclusion that in order to fit the observed profiles, a residual stress term is indeed necessary, and that a diffusion (D) and a pinch (V) model alone is not sufficient.[7–11] The idea that intrinsic rotation may be explained by a residual stress is quite general and is not necessarily limited to the particular mechanism of $E\times B$ shear-drive. The key effect of residual toroidal stress, emerges from a unified and systematic theory of radial transport of wave momentum and the processes of its exchange with particles. The theory includes resonant as well as nonresonant momentum transport and yields a pinch as well as a residual stress component. A general method to calculate the symmetry breaking mechanism without *a priori* assumptions has been developed.[12] Various mechanisms can give rise to residual stress such as toroidal current which generates directional asymmetry in growth rates (e.g., Ref. 13), $E\times B$ shear,[7,14] Elsasser population imbalance in Alfvénic turbulence,[15] charge separation induced by polarization drift,[16] up-down asymmetry of flux surfaces,[17] and the turbulence intensity profile itself. Here, since the focus is on H-mode plasmas, we consider $E\times B$ *shear as the primary symmetry breaking mechanism*. Note that a residual stress that relies on $E\times B$ shear can be shown to survive even in the presence of substantial turbulence suppression. This is mainly due to the fact that while both the diagonal and off-diagonal fluxes are reduced by $E\times B$ shear, the reduction in the residual toroidal stress component is weaker than the reduction in χ_ϕ.

The accumulated data on intrinsic rotation suggests that while its trigger is strongly localized in the pedestal, an additional mechanism is likely needed to produce peaked core profiles. This suggests that probably two mechanisms, one for the pedestal, and one for the core, together regulate tokamak rotation profiles. The particular mechanism of $E\times B$ shear-driven residual stress, cannot explain peaked profiles due to the fact that when it is efficient, it acts only in a narrow shear layer. Thus, to this end, a complementary theoretical path was also followed. Taking the parallel velocity moment of the conservative form of the gyrokinetic equations[18,19] in toroidal geometry, it was shown that magnetic curvature leads to a convective flux (i.e., a "pinch," if inward) of angular momentum density.[20] Afterwards, it was also pointed out that a part of this flux, the so called turbulent equipartition (TEP) pinch component, can also be obtained from simple consideration of angular momentum conservation in toroidal geometry.[21] This TEP pinch is always inward, regardless of the type of turbulence causing the mixing, and thus is the most robust momentum pinch mechanism. Note that a related mechanism of momentum pinch driven by the Coriolis drift in rotating frame has also been found for ion temperature gradient (ITG) driven instability.[22]

a)Electronic mail: ozgur.gurcan@lpp.polytechnique.fr.

 © 2010 American Institute of Physics

There has also been a series of numerical simulations[23–27] motivated by these observations and attempts for a theoretical explanation. However it seems that we are not yet at the stage where we can address the issue of intrinsic rotation as a self-organization phenomenon associated with the L-H transition using direct numerical simulations. However formulations that are able to evolve turbulence and flows simultaneously in the laboratory frame, while respecting the basic neoclassical underlying structure, may, in the near future, be able to tackle this difficult problem.[26,28,29]

Here, we also give a heuristic discussion of the general thermodynamical role of the pedestal in generating toroidal rotation. We note that within the formulation of residual stress, the pedestal acts as a heat engine and converts heating to mechanical (flow) energy through turbulent or wave mechanical processes. This occurs when the supplied heat (e.g., via the temperature gradient) drives microinstabilities, which have net wave momenta (e.g., due to strong $E\times B$ shear symmetry breaking in the pedestal). Since the wave momentum flux is part of the momentum flux of the plasma,[12] it follows that as wave momentum is transported, the plasma momentum must change locally. We note that this is a general and robust process, and it unmistakably links toroidal rotation physics to properties of the pedestal (e.g., the jump in temperature, etc.) while the efficiency of conversion (and possibly the direction of rotation) are set by the dynamics of microturbulence.

The remainder of the paper is organized as follows. In Sec. II, we introduce the model that we later use to derive analytically a scaling formula for the toroidal velocity with the pedestal width and show the same scaling by integrating the model numerically. In Sec. III, we explain the physics of intrinsic rotation by analogy to heat engine and note that a similar scaling follows from more general thermodynamic arguments. In Sec. IV we discuss these results and provide our conclusions.

II. THE MODEL

A simple minimal model, with sufficient degrees of freedom to capture established empirical trends with total stored energy and has the ability to produce both peaked and flat profiles, can be constructed by incorporating the two primary effects that are mentioned above (i.e., the TEP pinch and the $E\times B$ shear-driven residual stress). The simple transport model that we propose for this purpose consists of equations of continuity, heat transport and angular momentum transport:

$$\frac{\partial n}{\partial t}+\frac{1}{r}\frac{\partial}{\partial r}(r\Gamma_n)=S_n, \tag{1a}$$

$$\frac{\partial P}{\partial t}+\frac{1}{r}\frac{\partial}{\partial r}(rQ)=H, \tag{1b}$$

$$\frac{\partial L_\phi}{\partial t}+\frac{1}{r}\frac{\partial}{\partial r}(r\Pi_{r,\phi})=\tau_\phi. \tag{1c}$$

It is important to use angular momentum density in order to describe mean flow evolution since this quantity is globally conserved in the absence of radial currents or external torques. Angular momentum can then be related to the mean flow via a simple algebraic relation [see Eq. (3c)]. Note that, part of this "toroidal residual stress" comes from nonambipolar turbulent transport generating a radial current and therefore a $J\times B$ torque in the perpendicular (i.e., $\hat{\mathbf{r}}\times\hat{\mathbf{b}}$) direction-related to the perpendicular Reynolds stress.[30] A careful study of this effect is left to a future publication. Here we simply consider the case $\langle J_r\rangle=0$.

In Eqs. (1a)–(1c), the fluxes are given by

$$\Gamma_n=-D_0\frac{\partial n}{\partial r}-D_1\varepsilon\left(\frac{\partial n}{\partial r}+V_{rn}n\right), \tag{2a}$$

$$\Pi_{r,\phi}=-\nu_0\frac{\partial L_\phi}{\partial r}-\nu_1\varepsilon\left[\frac{\partial L_\phi}{\partial r}+V_{rL}L_\phi\right]+S, \tag{2b}$$

$$\text{where}\quad S=-\varepsilon\alpha(r)n(r)\left(1-\frac{\sigma}{P_0}\frac{\partial P}{\partial r}\right)\frac{\partial v_{Ey}}{\partial r}, \tag{2c}$$

$$Q=-\chi_0\frac{\partial P}{\partial r}-\chi_1\varepsilon\frac{\partial P}{\partial r}. \tag{2d}$$

We include a turbulent pinch for density (i.e., V_{rn}) as well as momentum (i.e., V_{rL}). Both of these terms can be understood as part of the same physical process: namely, the radial homogenization of the magnetically weighted variables,[20,21] where "magnetic weighting" arises due to the compressibility of the $E\times B$ drift in toroidal geometry. In practice, the magnitudes of these pinches are comparable, but not identical, since momentum is carried by passing ions, while the magnetically trapped electrons make a significant contribution to the particle flux. With these caveats in mind, we will usually use $V_r\equiv V_{rn}=V_{rL}$ to refer to both. Moreover, the total particle pinch and the total angular momentum pinch as derived in Ref. 20 contains additional terms, in particular a convective thermoelectric flux component, which we do not consider here. This component is usually in opposite directions for particles and angular momentum.

A crucial element in this simple model is the residual stress S. As mentioned previously, S could be due to a multitude of mechanisms. Since here the focus is on H-mode, we consider $E\times B$ shear as the primary source of symmetry breaking and so we take S to be proportional to the $E\times B$ shear.

The system is closed via the radial force balance equation, which relates $E\times B$ shear, pressure P, density n and momentum profiles. Here we take $v_\theta\approx 0$, due to strong parallel neoclassical damping. This need not always be true in the case of strongly anomalous transport and high temperature, and the effects of turbulence driven poloidal rotation merit further study. We also neglect the feedback of toroidal rotation from the $v_\phi B_\theta$ term and use a reduced version of the radial force balance, mainly for simplicity. We note that the

turbulence is suppressed by the sheared $E\times B$ flow,[31] which we describe by a simple shear suppression formula, as in Ref. 32. Also, finally we relate the flux surface average of the flow to angular momentum:

$$\frac{\partial v_{Ey}}{\partial r} = \left(\frac{\rho_*}{n_0 P_0}\right)\frac{\partial n}{\partial r}\frac{\partial P}{\partial r} + \cdots, \tag{3a}$$

$$\varepsilon = \frac{\varepsilon_0}{[1+\beta(\partial v_{Ey}/\partial r)^2]}, \tag{3b}$$

$$v_\phi(r,t) = \left[\frac{L_\phi(r,t)}{n(r,t)}\right]\lambda_2(r). \tag{3c}$$

We also impose the boundary conditions:

$$L_\phi(a) = v_\phi(a) = P(a) = 0,$$

$$n(a) = n_a.$$

Note that, since this is a model of momentum transport in the "core" that includes the pedestal, here a actually corresponds to the last closed flux surface. The assumption of simple no-slip boundary condition may not in general, be realistic. This is especially true for the case of strong scrape-off layer (SOL) flows,[33] comparable to intrinsic rotation. However we expect that in H-mode, $E\times B$ shearing to sever the link between the poloidally asymmetric SOL flows and the intrinsic core rotation, thus simplifying the boundary condition. The effect of adding a constant v_{SOL} as a boundary condition on the model given above [i.e., $v_\phi(a)=v_{\mathrm{SOL}}$] is to offset the pedestal flow by this added boundary flow. In reality, since there is substantial intrinsic core rotation in the H-mode case, a fully self-consistent treatment of the evolution requires dynamical matching of stresses rather than treating one region as a fixed boundary condition for the other. Such an analysis is left to a future study,

We evolve $n(r,t)$, $P(r,t)$, and $L_\phi(r,t)$. The parameters of the model are D_0, D_1, ν_0, ν_1, χ_0, χ_1, α, β, ρ_*, and V_r (with β not to be confused with the usual plasma β). The observables are $v_\phi(r,t)$, $n(r,t)$, and $P(r,t)$. Note that the boundary conditions are associated only with the evolving fields and that there is no separate boundary condition, for example, for v_{Ey}. The functional forms of $\lambda_2(r)$ and $\lambda_1(r)$ define the geometry associated with magnetic field inhomogeneity and thus determine the TEP pinch. In general, $V_r=-\lambda_1(\partial/\partial r)(\lambda_1^{-1})$ where λ_1 is defined implicitly via $\nabla\cdot(\mathbf{v}_E\lambda_1)=0$. In practice this gives $V_r\sim -2a/R$ for $\lambda_1\approx B^2$. Equation (3c) gives the flux surface averaged flow in terms of flux surface averaged angular momentum where $\lambda_2=\langle R\rangle/\langle R^2\rangle$. Here we take $|V_r|\lesssim 1$ and $\lambda_2(r)\approx(1-r^2/R_0^2)/R_0$ assuming $r/R_0<1$. Similarly, since S was originally computed for $\langle v_\parallel\rangle$, in order to use it for $\langle L_\phi\rangle$, we multiply it by $n\langle R\rangle$, which gives $\alpha(r)\propto(1+r^2/R_0^2)R_0\alpha_0$. Normalizing $L_\phi\to L_\phi/n_{\mathrm{ref}}c_sR_0$, we can use the normalized coefficients $\lambda_2(r)\approx(1-r^2/R_0^2)$ and $\alpha(r)\propto(1+r^2/R_0^2)\alpha_0$. Here, the linear ITG driven case corresponds to α_0 positive, σ negative (with $|\sigma|<1$). Note that $\sigma\propto\omega/\gamma^2$ in the limit $\gamma\gg\omega$, the fluid ITG limit for which the mode shift is computed. Interestingly however, in the nonlinear limit, the turbulence decorrelation in ITG is dominated by the fluctuating $E\times B$ velocity. In this limit, one uses $i\tau_{ck}/\omega_k$ instead of the quasilinear i/ω_k^2. This results in $\alpha_0>0$ and $\sigma>0$, equivalent to the case previously studied in Ref. 7.[40] This is one of the cases we consider here as well. Apparently, this case (i.e., one with ITG, Doppler shifted to electron direction) gives corotation profiles with favorable scaling with pedestal width.

Nevertheless, here we study both of these cases (i.e., $\sigma\lessgtr 0$) to note different conditions for corotation and scaling. We note that the sign of the coefficients as computed by quasilinear theory is not a robust feature of the flux, in particular, it depends on the cross-phase between Φ and P, which in turn is affected by the existence of large scale structures. Thus we suggest that the direction of the off-diagonal momentum flux, and in particular, its dependence on the existence of large scale structures, such as zonal flows, should be studied using direct numerical simulations that can address momentum transport self-consistently.

The set of Eqs. (1a) and (3c) reproduces the well-known model of Ref. 32 with the addition of nondiffusive angular momentum evolution (also similar to Ref. 14). Here the focus is H-mode pedestal, and internal transport barrier effects on rotation are thus excluded. Therefore a reduced form of the force balance is used such that there is *no feedback* on density and/or pressure evolution by the angular momentum (i.e., since the rotation is intrinsic, $E_r\approx\nabla_r P/n$). In this limit, we recover dynamics qualitatively very similar to previous results.[7] Noticeable differences are due to the ratio r/R_0, which modify the functional forms of $\lambda_2(r)$ and $\alpha(r)$ and measure the importance of the toroidal moment of inertia effect and the dimensionless TEP pinch V_r [e.g., as in Eq. (2a)], which reflect the relative strength of anomalous pinch to anomalous diffusion. Note that we mostly focus on the case $\nu_1/D_1=1$.

A. Scaling of velocity with pedestal width

An analytical estimation for the flow velocity can be made by assuming simple piece-wise linear functional forms for pressure and density profiles and using the stationarity condition $\Pi_{r,\phi}=0$ on Eq. (2b). In order to study basic scalings, we choose a simple form for the profiles:

$$n \sim n_{\mathrm{ped}} - (n_0 - n_{\mathrm{ped}})\left(\frac{x}{a-w}\right)\Theta(-x) - n_{\mathrm{ped}}\left(\frac{x}{w}\right)\Theta(x), \tag{4}$$

where $x\equiv r-(a-w)$ is the distance from the profile "corner," (e.g., see Fig. 1) $\Theta(x)$ is the Heaviside step function and expressions for pressure and angular momentum profiles are formed similarly. The forms of the profiles imply that $v'_{Ey}(r)$ is large in the "pedestal region" [i.e., roughly $v'_{Ey}(r_>)\approx\rho_*/w^2$], and small otherwise. Also assuming $w\ll 1$, we can estimate the pedestal flow speed, as

$$v_{\mathrm{ped}} \propto \left(\frac{\alpha_0\varepsilon_0\sigma}{\nu_0\beta\rho_*}\right)\left(\frac{w}{n_{\mathrm{ped}}}\right)w. \tag{5}$$

In fact defining $A^{-1}\equiv dn_{\mathrm{ped}}/dw$, with the assumption that the n_{ped} also scales in this range with w—in accord with what we observe from the model—we get

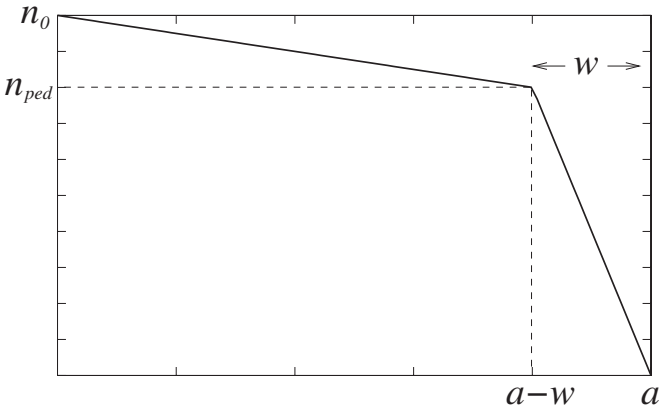

FIG. 1. Analytical equilibrium profiles used for estimation [i.e., Eq. (4)].

$$v_{\mathrm{ped}} \propto A\left(\frac{\alpha_0\varepsilon_0\sigma}{\nu_0\beta\rho_*}\right)w. \tag{6}$$

Furthermore, a similar expression in the case of $\sigma \approx 0$ can be derived, which is in fact w/σ times Eq. (6).

Using $|L_s^{-1}| \to \hat{s}/qR$, and the results from Ref. 7: $|\alpha_0| \sim \nu_1(\rho_*/\tau)(L_n\hat{s}/qR)$, and $|\sigma| \sim \rho_* c_s k_y \tau_c$, gives $(\alpha_0\varepsilon_0\sigma/\nu_0) \sim (\epsilon\hat{s}/q)(\nu_1\varepsilon_0/\nu_0)$, and the shear reduction coefficient is roughly $\beta \sim c_s^2 k_y^2 r_c^2/a^2\gamma^2$. Here the normalizations are $r \to r/a$ (i.e., $w \to w/a$) and $v_\phi \to v_\phi/c_s$. Here $\nu_1\varepsilon_0/\nu_0$ is the ratio of turbulent to neoclassical or residual turbulent transport coefficients such that $\nu_1\varepsilon_0/\nu_0 \to D_{\{B,GB\}}/D_{\{\mathrm{neo,res}\}}$. This coefficient can be quite large. If we use the standard mixing length estimate, leaving r_c and τ_c unspecified, i.e., $\gamma \to \tau_c^{-1}$, $\nu_1\varepsilon_0 \to r_c^2/\tau_c$ we obtain

$$\delta v_\phi \sim c_s\left(\frac{\rho_*\epsilon\hat{s}}{\tau q}\right)\left(\frac{a^2/\tau_c}{D_{\{\mathrm{neo,res}\}}}\right)\left(\frac{c_s^{-1}k_y^{-1}}{\tau_c}\right)\left(\frac{L_n L_{n,\mathrm{ped}}}{a^2}\right)\left(\frac{w}{a}\right). \tag{7}$$

where $L_{n,\mathrm{ped}}^{-1} \equiv (1/n_0)(dn_{\mathrm{ped}}/dw)$ (in fact, the coefficient of linear regression of n_{ped}/n_0 versus w) and n_0 is a fixed reference density. Note that in a narrow region, such as the pedestal, diffusion and residual stress effects are likely to be dominant over a TEP pinch. Thus, the neglect of the pinch in the above analytical estimate is justified as long as the pedestal is narrow, but not too narrow as to render the piecewise linear approximation invalid. Yet, the above scaling is expected to be valid in a range of relevant pedestal widths.

Although Eq. (5) gives us an estimate of the pedestal flow velocity, this does not translate directly into an on-axis flow velocity. If the pedestal height is small, than it is the rest of the profile that determines the on-axis component, which actually increases as w decreases (along with decreasing P_{ped}). However for the pedestal velocity itself, Eq. (5) is a reasonable approximation. Also, up to the point where $(P_0 - P_{\mathrm{ped}}) > P_{\mathrm{ped}}$, the trend may be expected to approximate the behavior of the on-axis flow speed.

B. Numerical studies

We have also studied this model numerically, results of which can be found in Figs. 2–5. Since the model equations are very simple, extensive scans of the parameter space have been performed, and we note that there are parameter regimes which are exceptions to the general trends presented here. Furthermore, since the model is overly simple, we did not try to use experimental estimates for the parameter values. Nevertheless, agreement between the numerical integration and the above analytical estimate can be seen clearly in figure. This suggests that the analytical estimate can be used as a general rule of thumb for estimating the velocity at the top pedestal.

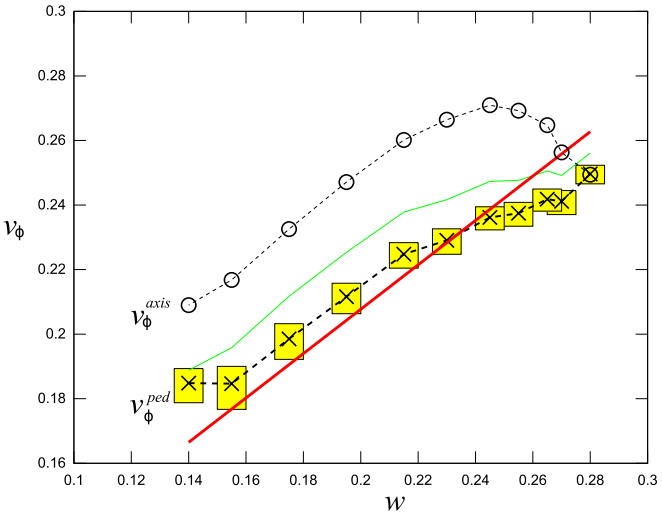

FIG. 2. (Color online) Pedestal velocity v_ϕ^{ped} vs the pedestal width w. Here, the crosses correspond to the numerical integration of the model, with boxes around them defining the error bars corresponding to finite numerical resolution. Circles denote the values of the corresponding on-axis velocities. The thick solid line (red) is the analytical estimate of the slope [e.g., Eq. (6)], the thin solid line (green) is the analytical estimate [e.g., Eq. (5)] using w/n_{ped} from the numerical scan. The scan is done by changing η, the inverse fueling depth, by recording the resulting pedestal height and widths. The values of the parameters correspond to $D_0=\chi_0=\nu_0=2$, $D_1=\chi_1=\nu_1=\alpha_0=4$, $\sigma=4$, $\gamma_a=6$, $q_a=40$, $\lambda=10$, $\rho_*=0.1$, $R/a=10$, $\varepsilon_0=1$, and $V_r=0$. The parameters are chosen in particular to allow a wide w scan.

Note that within this simple model, it is η, the inverse fueling depth (i.e., $S_n \sim \Gamma_a e^{-\eta[n_a(r-a)+n_a'(r-a)^2/2]}$), which primarily determines the pedestal width, and the size of the pedestal change, (when η is changed). Here we give the result in terms of a proportionality of the toroidal flow velocity with the pedestal width. However, during a scan of η, we also observe that $w \propto \{n_{\mathrm{ped}}, P_{\mathrm{ped}}\}$, and the form of our result for the velocity depends on this height scaling. This could be improved by including a gradient in χ *a la* Ref. 34. However determination of the pedestal width to height scaling is beyond the scope of this paper.

Similar width scans have also been performed in the presence of a strong inward TEP pinch as shown in Fig. 3. As a result of the pinch, the angular momentum and flow profiles become peaked on axis. However as the pedestal width is increased, the density profile becomes more and more peaked in comparison with the angular momentum profile. This is in fact an artifact of the method we use to change the width by changing η. As η is decreased the total particle source is increased which allows more particles to be carried inward by the pinch. When the density is more peaked the flow profile becomes less peaked. However, the on-axis an-

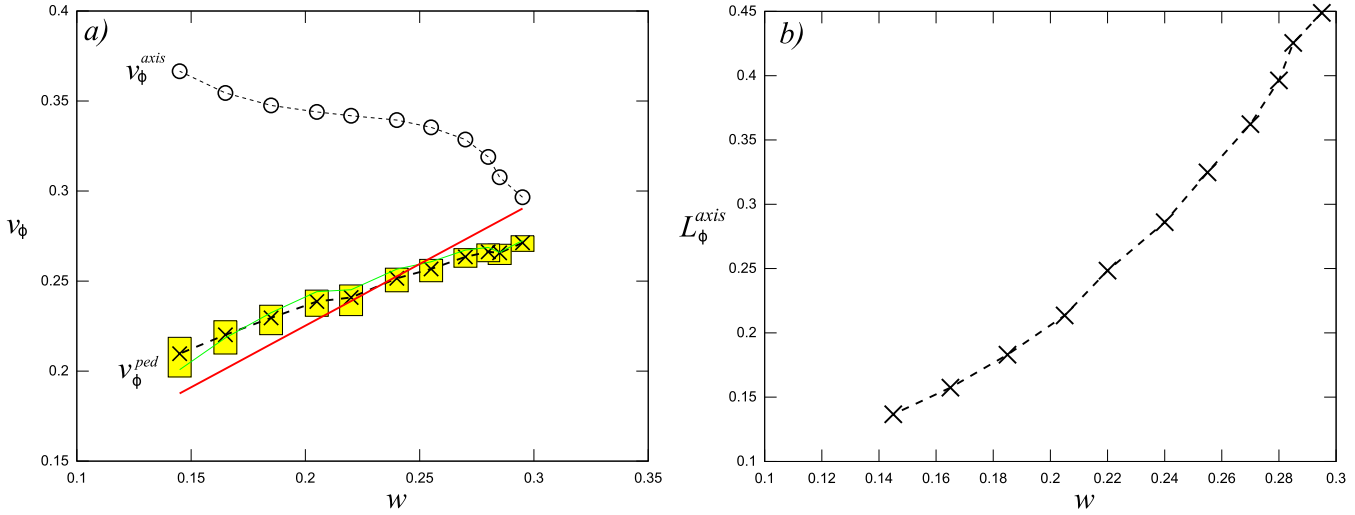

FIG. 3. (Color online) Pedestal velocity v_ϕ^{ped} vs the pedestal width w in the presence of a TEP pinch. The legend and the parameter values are as described in Fig. 2. The only difference is that here $V_r=-0.5$ (which is rather large). Note that the pinch is applied to both the angular momentum and density and v_ϕ is computed using Eq. (3c). The flow on-axis decreases because the density profile becomes more peaked than the angular momentum profile. Note also that when compared with Fig. 2, the slope of the pedestal scaling is slightly reduced in the presence of a large inward pinch of angular momentum.

gular momentum density, which is in fact the conserved quantity, increases in absolute terms as the pedestal width is increased.

III. TURBULENCE AS A HEAT ENGINE: A MODEL FOR INTRINSIC ROTATION

A heat engine is a device that converts heat to mechanical energy, using some kind of cyclic motion driven by temperature gradients. Based on this definition, the analogy with the phenomenon of intrinsic rotation is obvious. A heat engine requires a hot region as the source of heat and a cold region as the sink, thus generating a heat flow or flux. In an H-mode plasma, by taking the top of the pedestal as the "hot region" and the bottom of the pedestal, as the "cold region," we can think of the pedestal as a heat engine (see Fig. 6).

In order to elaborate this analogy, let us consider Eq. (1b). Assuming that the heat source is localized in the core region, we can integrate Eq. (1b) over the pedestal as

$$\frac{d}{dt}\int_{\text{ped}} (nT)d^3x = Q_{\text{ped}} - Q_a,$$

where we defined the total heat flux from the core into the pedestal as $Q_{\text{ped}}=\int Q(r_{\text{ped}})dS$, and the total heat flux from the pedestal to the SOL as $Q_a=\int Q(a)dS$ and dS is the surface element (i.e., $dS=rRd\phi d\theta$ for a simple circular plasma). These two would normally be the same during either L-mode or H-mode operation. However during the L-H transition we can have $Q_{\text{ped}}>Q_a$. The total heat absorbed by the pedestal

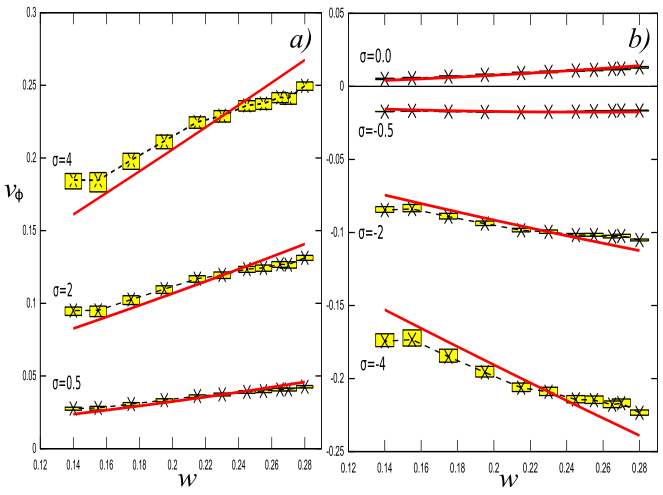

FIG. 4. (Color online) Pedestal velocity v_ϕ^{ped} vs the pedestal width w. As in Fig. 2, the crosses correspond to the numerical integration of the model, with boxes around them defining the error bars corresponding to finite numerical resolution, and the thick solid line (red) correspond to the analytical estimate of the slope [e.g., Eq. (6)]. The parameters are also the same as in Fig. 2, except σ values which are denoted in the figure.

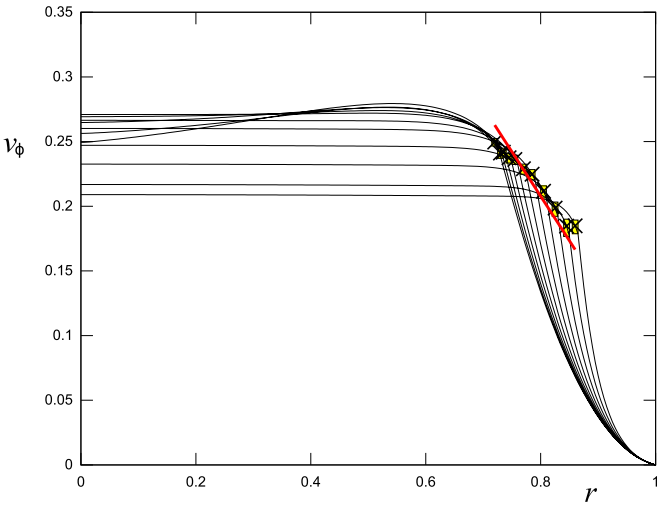

FIG. 5. (Color online) Velocity profiles during the scan in Fig. 2. Note that, while of course the parameters, such as, $\alpha_0, \sigma, \mu, \beta, \nu_1, \nu_0$ etc. are important, assuming these are fixed, the pedestal width defines the toroidal flow velocity at the top of the pedestal.

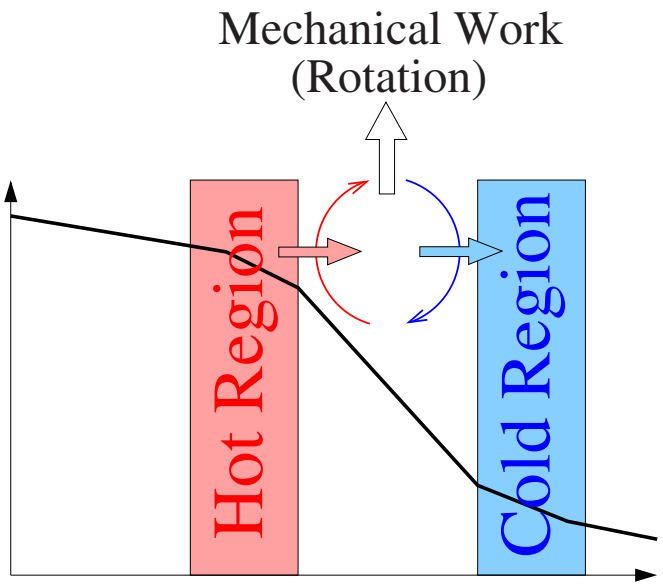

FIG. 6. (Color online) The parallel between heat engine and intrinsic rotation.

during the L-H transition is equal to the "maximum" energy available to drive flows during the L-H transition.

We can also introduce entropy production rates corresponding to various elements of this system as

$$\dot{S}_{\text{plasma}} = \dot{S}_{\text{core}} + \dot{S}_{\text{ped}} + \dot{S}_{\text{SOL}}, \tag{8}$$

so that $Q_{\text{ped}} = -T_{\text{ped}}\dot{S}_{\text{core}}$, $Q_a = T_a\dot{S}_{\text{SOL}}$ and $\dot{S}_{\text{ped}}$ is the entropy production inside the pedestal (note that we use plasma physics-like notation where Q is heat flux). In other words, in this idealized partition, while the entropy of the core decreases (as it loses heat), entropy of the edge increases (as it absorbs heat), the total entropy of the plasma, in the end, has to increase (the formulation here parallels that of Ref. 35). During the L-H transition $Q_{\text{ped}} > Q_a$, (or in other words, $Q_a = Q_{\text{ped}} - \Delta\dot{W} < Q_{\text{ped}}$). In this case, we can write Eq. (8) as

$$\dot{S}_{\text{plasma}} = \frac{Q_{\text{ped}} - \Delta\dot{W}_{\text{ped}}}{T_a} - \frac{Q_{\text{ped}}}{T_{\text{ped}}} + \dot{S}_{\text{ped}},$$

since by the 2nd law of thermodynamics this must be greater than zero, we find that the maximum possible work that can be extracted from this system per second is

$$\Delta\dot{W}_{\text{ped}} \le Q_{\text{ped}}\left(1 - \frac{T_a}{T_{\text{ped}}}\right). \tag{9}$$

This is the Carnot efficiency of an ideal heat engine [i.e., $(T_{\text{hot}} - T_{\text{cold}})/T_{\text{hot}} = W_{\text{mech}}/W_{\text{app.}}$]. However, in practice, even in a carefully designed heat engine, not all of this free energy is available to drive flows. In the case of the pedestal, only a fraction of this available free energy can be converted into mechanical energy (i.e., flows) by turbulent motions. Furthermore, a part of this energy will be directly conducted to the SOL, and thus will not be available for driving rotation. In steady state, the excess power that goes to drive flows in the pedestal vanishes, leading to the pure conduction result

$$\dot{S}_{\text{plasma}} = \frac{Q_{\text{ped}}}{T_a}\left(1 - \frac{T_a}{T_{\text{ped}}}\right) \ge 0.$$

However since the flows persist in the presence of dissipation, this suggests a balance such that the free energy that is supplied to the pedestal from the core is being used to drive turbulence, which generates mesoscale flow shears (i.e., zonal $E \times B$ flows), which then allow the turbulence to drive toroidal flow by the $E \times B$ shear-driven residual stress, however the $E \times B$ shear also scatters the turbulence to higher wave-numbers leading to a dissipation of turbulence, and thus depletion of the source for its own drive (as well as that of toroidal flow). A steady state can be reached when the depletion of the drive of large scale flows reduce to levels comparable to the neoclassical flow damping. It is well known however systems such as these may display intermittent dynamics as well as going to a steady state.

While a full L-H transition model can be formulated based on this approach and the maximum entropy principle,[36] our purpose here is simply to connect the temperature pedestal height to the resulting pedestal velocity height. For a simple estimate of this effect, let us consider the angular momentum flux

$$\Pi_{r,\phi} = \chi_\phi m_i n_{\text{ped}} R \frac{V_{\text{ped}}}{w} + S(\Delta\dot{w}), \tag{10}$$

where $S(\Delta\dot{w})$ is the residual stress, taken to be a function of the available mechanical power (we further assumed $V_0 = 0$ at the edge for simplicity). In the absence of external torque input and edge flows, the steady state implies a balance between diffusive and residual components of the angular momentum flux. Here, while Eq. (9) gives the available power, the balance in Eq. (10) sets the direction of rotation,

$$V_{\text{ped}} = \frac{w}{\chi_\phi m_i n_{\text{ped}} R} S(\Delta\dot{w}),$$

which is positive if $S(\Delta\dot{w}) > 0$. The flow energy driven by the residual stress (i.e., S) is

$$\dot{W}_{\text{res}} = \int_{\text{ped}} \left[\frac{\partial v_\phi}{\partial r}\frac{S}{R}\right] d^3x, \tag{11}$$

expected to be the same as $\Delta\dot{w}$, which gives

$$S(\Delta\dot{w}_{\text{ped}}) = s\frac{n_{\text{ped}} R}{|V_{\text{ped}}|}\Delta\dot{w}_{\text{ped}}, \tag{12}$$

where s is a "turbulent transport coefficient" of residual stress whose sign sets the direction of the flow. At this point, one is again challenged with the question of the origin symmetry breaking and has to confront microturbulence characteristics in order to answer it. However we note that, the existence of a pedestal (and thus $E \times B$ shear, which is taken for granted in this simple picture), already guarantees broken symmetry. Using Eq. (12), we obtain

$$V_{\text{ped}}^2 = w\frac{|s|}{\chi_\phi m_i} Q_{\text{ped}}\left(\frac{T_{\text{ped}} - T_a}{T_{\text{ped}}}\right). \tag{13}$$

From the perspective given in this section and particularly Eq. (13), one can view Rice's scaling with plasma en-

ergy as a global scaling of mechanical work (i.e., plasma rotation) with the work done on the system by heating. The dependence on other parameters (such as the inverse scaling with plasma current) would influence this relation by changing the efficiency of the conversion, or by modifying the available free energy. This is particularly the case for the parameters that simply modify the pedestal width. For instance the inverse scaling of the pedestal width with current [through β_θ as in Ref. 37, where $\beta_\theta = 8\pi\langle P\rangle / B_\theta^2 \approx \int P dS \times (2c^2/I^2)$], carries over to toroidal rotation as argued in Ref. 11. Basically, *increasing the current makes the heat engine smaller and so reduces its efficiency*. Finally, if we use $Q_{\mathrm{ped}} = \chi_i (T_{\mathrm{ped}} - T_a)/w$, we get

$$|V_{\mathrm{ped}}| = (T_{\mathrm{ped}} - T_a)\sqrt{\frac{|s|}{m_i T_{\mathrm{ped}}}\frac{\chi_i}{\chi_\phi}}.$$

IV. RESULTS AND DISCUSSION

A clarification should be made in order to compare our model with experiment. Here, all the figures correspond to the nondimensional pedestal velocity, v_ϕ/c_s for which a scaling of the form $v_\phi/c_s \propto (w_{\mathrm{ped}}/a)$ is predicted using dimensional analysis and numerical integration of the model. We argue that the pedestal flow accounts for most of this intrinsic rotation. Taking this result literally and noting that $w/a \propto n_{\mathrm{ped}}/n_0$ for an η scan in this model, we obtain

$$v_\phi \sim C\left(\frac{w}{a}\right)c_s, \tag{14}$$

where the plasma stored energy (i.e., $W_p = \int nTdV_p$), V_p being plasma volume, naturally scales with the pedestal width. Furthermore, C as defined in Eq. (14) is not a simple constant. As can be seen in Eq. (7), $C \sim (\rho_* \epsilon \hat{s}/\tau q)(a^2/D_{\{\mathrm{neo,res}\}}\tau_c) \times (c_s^{-1}k_y^{-1}/\tau_c)(L_n L_{n,\mathrm{ped}}/a^2)$, which implies more complicated dependencies than the simple scaling of Eq. (14). The reason we write Eq. (14) in this form, is to note that a pure width scaling corresponds (to some extent) to the scaling that has experimentally been observed.

The Rice scaling is of the form $v_\phi \propto W_p/I_p$. Thus, Eq. (14) suggests both a basic agreement with stored energy dependence of the Rice scaling as well as some additional scalings which may impact the extrapolation to ITER, in particular via ρ_* and ϵ dependences in the coefficient C above. We admit strong dependence of these results on assumptions about fluctuation characteristics within the pedestal region (i.e., Bohm versus gyro-Bohm) especially through τ_c. We should also note that the Rice scaling is for the flow on axis, whereas the analytical scaling with w, which we devise here, is for the velocity at the top of the pedestal. These two may differ strongly if the pinch is sufficiently strong.

In this paper, we have introduced a simple model of the H-mode intrinsic rotation, which combines both the $E\times B$ shear-driven residual stress, and the TEP pinch. We note that the model predicts a simple scaling of rotation velocity with the pedestal width w. This is a clear, testable prediction, in rough agreement with several aspects of the Rice scaling.[5] It is also a signature of the symmetry breaking mechanism based on $E\times B$ shear-driven residual stress in H-mode plasmas.

ACKNOWLEDGMENTS

We thank (in alphabetical order) K.H. Burrell, C.S. Chang, J. deGrassie, X. Garbet, M. Greenwald, C. Hidalgo, K. Ida, K. Itoh, S.-I. Itoh, Y. Kamada, S. Kaye, J. Rice, W. Solomon, W. Wang, and M. Yoshida for many stimulating discussions. This research was supported by Department of Energy Contract No. DE-FC02-08ER54959 (UCSD) and U.S. Department of Energy Contract No. DE-AC02-09-CH11466 (PPPL) and the Agence Nationale de la Recherche, Contract No. 06-3_134975.

[1] J. E. Rice, W. D. Lee, E. S. Marmar, P. T. Bonoli, R. S. Granetz, M. J. Greenwald, A. E. Hubbard, I. H. Hutchinson, J. H. Irby, Y. Lin, D. Mosseissian, J. A. Snipes, S. M. Wolfe, and S. J. Wukitch, Nucl. Fusion **44**, 379 (2004).
[2] M. Yoshida, Y. Koide, H. Takenaga, H. Urano, N. Oyama, K. Kamiya, Y. Sakamoto, and Y. Kamada, Plasma Phys. Controlled Fusion **48**, 1673 (2006).
[3] A. Bortolon, B. P. Duval, A. Pochelon, and A. Scarabosio, Phys. Rev. Lett. **97**, 235003 (2006).
[4] J. S. deGrassie, J. E. Rice, K. H. Burrell, R. J. Groebner, and W. M. Solomon, Phys. Plasmas **14**, 056115 (2007).
[5] J. E. Rice, E. S. Marmar, P. T. Bonoli, R. S. Granetz, M. J. Greenwald, A. E. Hubbard, J. W. Hughes, I. H. Hutchinson, J. H. Irby, B. LaBombard, W. D. Lee, Y. Lin, D. Mossessian, J. A. Snipes, S. M. Wolfe, and S. J. Wukitch, Fusion. Sci. Technol. **51**, 288 (2007).
[6] Y. Kamada, M. Yoshida, Y. Sakamoto, Y. Koide, N. Oyama, H. Urano, K. Kamiya, T. Suzuki, A. Isayama, and the JT-60 Team, Nuclear Fusion **49**, 095014 (2009).
[7] Ö. D. Gürcan, P. H. Diamond, T. S. Hahm, and R. Singh, Phys. Plasmas **14**, 042306 (2007).
[8] W. M. Solomon, K. H. Burrell, J. S. deGrassie, R. Budny, R. J. Groebner, J. E. Kinsey, G. J. Kramer, T. C. Luce, M. A. Makowski, D. Mikkelsen, R. Nazikian, C. C. Petty, P. A. Politzer, S. D. Scott, M. A. Van Zeeland, and M. C. Zarnstorff, Plasma Phys. Controlled Fusion **49**, B313 (2007).
[9] B. P. Duval, A. Bortolon, A. Karpushov, R. A. Pitts, A. Pochelon, O. Sauter, A. Scarabosio, G. Turri, and the TCV Team, Phys. Plasmas **15**, 056113 (2008).
[10] M. Yoshinuma, K. Ida, M. Yokoyama, K. Nagaoka, M. Osakabe, and the LHD Experimental Group, Nucl. Fusion **49**, 075036 (2009).
[11] P. H. Diamond, C. J. McDevitt, Ö. D. Gürcan, T. S. Hahm, W. X. Wang, E. S. Yoon, I. Holod, Z. Lin, V. Naulin, and R. Singh, Nucl. Fusion **49**, 045002 (2009).
[12] P. H. Diamond, C. J. McDevitt, O. D. Gürcan, T. S. Hahm, and V. Naulin, Phys. Plasmas **15**, 012303 (2008).
[13] T. E. Stringer, J. Nucl. Energy C, **6**, 267 (1964).
[14] R. R. Dominguez and G. M. Staebler, Phys. Fluids B **5**, 3876 (1993).
[15] C. J. McDevitt and P. H. Diamond, Phys. Plasmas **16**, 012301 (2009).
[16] C. J. McDevitt, P. H. Diamond, O. D. Gürcan, and T. S. Hahm, Phys. Plasmas **16**, 052302 (2009).
[17] Y. Camenen, A. G. Peeters, C. Angioni, F. J. Casson, W. A. Hornsby, A. P. Snodin, and D. Strintzi, Phys. Rev. Lett. **102**, 125001 (2009).
[18] T. S. Hahm, Phys. Fluids **31**, 2670 (1988).
[19] T. S. Hahm, Phys. Plasmas **3**, 4658 (1996).
[20] T. S. Hahm, P. H. Diamond, O. D. Gurcan, and G. Rewoldt, Phys. Plasmas **14**, 072302 (2007).
[21] Ö. D. Gürcan, P. H. Diamond, and T. S. Hahm, Phys. Rev. Lett. **100**, 135001 (2008).
[22] A. G. Peeters, C. Angioni, and D. Strintzi, Phys. Rev. Lett. **98**, 265003 (2007).
[23] C. S. Chang and S. Ku, Phys. Plasmas **15**, 062510 (2008).
[24] I. Holod and Z. Lin, Phys. Plasmas **15**, 092302 (2008).
[25] W. X. Wang, T. S. Hahm, S. Ethier, G. Rewoldt, W. W. Lee, W. M. Tang, S. M. Kaye, and P. H. Diamond, Phys. Rev. Lett. **102**, 035005 (2009).
[26] Y. Idomura, H. Urano, N. Aiba, and S. Tokuda, Nucl. Fusion **49**, 065029 (2009).

[27]F. J. Casson, A. G. Peeters, Y. Camenen, W. A. Hornsby, A. P. Snodin, D. Strintzi, and G. Szepesi, Phys. Plasmas **16**, 092303 (2009).
[28]G. Dif-Pradalier, V. Grandgirard, Y. Sarazin, X. Garbet, and P. Ghendrih, Phys. Rev. Lett. **103**, 065002 (2009).
[29]C. S. Chang, S. Ku, P. H. Diamond, Z. Lin, S. Parker, T. S. Hahm, and N. Samatova, Phys. Plasmas **16**, 056108 (2009).
[30]P. H. Diamond and Y.-B. Kim, Phys. Fluids B **3**, 1626 (1991).
[31]H. Biglari, P. H. Diamond, and P. W. Terry, Phys. Fluids B **2**, 1 (1990).
[32]F. L. Hinton and G. M. Staebler, Phys. Fluids B **5**, 1281 (1993).
[33]B. LaBombard, J. E. Rice, A. E. Hubbard, J. W. Hughes, M. Greenwald, R. S. Granetz, J. H. Irby, Y. Lin, B. Lipschultz, E. S. Marmar, K. Marr, D. Mossessian, R. Parker, W. Rowan, N. Smick, J. A. Snipes, J. L. Terry, S. M. Wolfe, and S. J. Wukitch, Phys. Plasmas **12**, 056111 (2005).
[34]M. A. Malkov and P. H. Diamond, Phys. Plasmas **15**, 122301 (2008).
[35]H. Ozawa, A. Ohmura, R. Lorenz, and T. Pujol, Rev. Geophys. **41**, 1018 (2003).
[36]Z. Yoshida and S. M. Mahajan, Phys. Plasmas **15**, 032307 (2008).
[37]P. B. Snyder, R. J. Groebner, A. W. Leonard, T. H. Osborne, and H. R. Wilson, Phys. Plasmas **16**, 056118 (2009).
[38]W. Horton, Rev. Mod. Phys. **71**, 735 (1999).
[39]P. W. Terry, Rev. Mod. Phys. **72**, 109 (2000).
[40]We note that the magnetic shear sign convention in Ref. 7 is nonstandard (i.e., in this paper, $k_\parallel = k_y x / L_s$, with $L_s^{-1} = \hat{s}/qR$ was used). Apparently this is a rather common, nonstandard convention (see for instance Ref. 38 Eq. 43, or Ref. 39 Eq. 5.4). This, combined with a possible typographical error, lead to parameter values which do not reflect the intended linear ITG case (while the drift wave case seems correct) in that paper. As we note, the linear ITG case corresponds to α_0 positive, σ negative (with $|\sigma| < 1$), with the sign convention that is used here.